Angewandte Chemie
Eine Zeitschrift der Gesellschaft Deutscher Chemiker

Supporting Information

Irreversible Conversion of a Water–Ethanol Solution into an Organized Two-Dimensional Network of Alternating Supramolecular Units in a Hydrophobic Zeolite under Pressure

*Rossella Arletti, Ettore Fois, Lara Gigli, Giovanna Vezzalini, Simona Quartieri, and Gloria Tabacchi**

anie_201610949_sm_miscellaneous_information.pdf

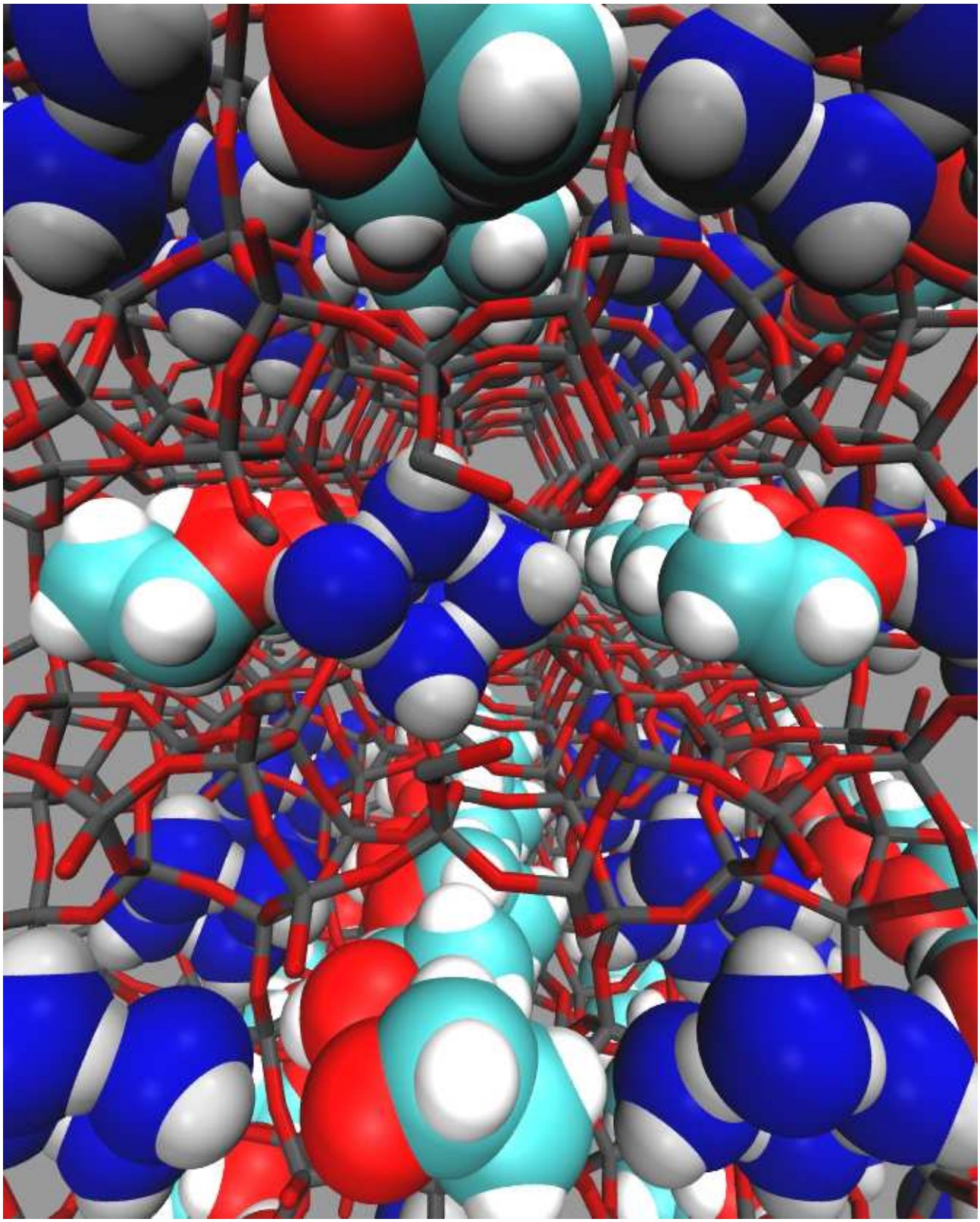

Contents:

1. ***Experimental methods and data analysis***
    - *1.1. Synthesis and characterization*
    - *1.2. XRPD experiments at high pressure*
2. ***Computational methods and models***
3. ***Additional computational results***
    - *3.1. Results of First Principles Molecular Dynamics simulations*
    - *3.2. Discussion of the results of First Principles Molecular Dynamics simulations*
    - *3.3. Graphical representation of the water clusters in Si-FER.*
4. ***General discussion on our findings, open questions, and perspectives***
    - *4.1. Role of the maximum applied pressure and of the pressure medium*
    - *4.2. Role of the topology and chemical composition of the framework*

References

1 EXPERIMENTAL METHODS AND DATA ANALYSIS

Ferrierite (framework type FER[1]) is both a well-known zeolite mineral[2,3] and a synthetic porous material, prepared readily by both aqueous[4] and non-aqueous routes.[5] Its crystal structure[6,7,8] is built up of rings of five SiO_4 tetrahedra (known as 5MR building units), which form layers on the *ab* plane. The layers are connected to form 10MR channels running parallel to [001] (*c*-axis), which are intersected by 8MR channels parallel to the [010] direction (*b*-axis). Six-membered rings connect the 10MRs channels along [010]. The structure contains cavities known as FER cages, formed by the intersection of the eight-membered ring channels and the six-membered ring channels (parallel to the *c*-axis). A graphical representation of the Si-FER framework, evidencing the section of the 8MR, 6MR and 10MR channels is depicted in Figure 4a-b of the main text.

1.1 Synthesis and characterization

The synthesis and the characterization of the all-silica ferrierite Si-FER was performed as described in Ref. (9a), to which the reader is referred for further details. To determine the chemical composition of the sample, a Cameca SX 50 Electron microprobe (experimental conditions: 20 kV, beam current 2 nA) was employed on a pellet of the zeolite powder using natural minerals as standards. The thermogravimetric analysis was carried out in air on 9.62 mg of sample, by operating at a 10 °C/min heating rate from room temperature to 900 °C. The weight loss (lower than 0.5 wt.%) indicated that all the template agents used in the synthesis [i.e. pyridine (C_5H_5N) and propylamine –(n-C_3H_9N)] were removed from the zeolite channels. The resulting chemical formula was [$Si_{36}O_{72}$].

1.2 XRPD experiments at high pressure

The in situ high-pressure (HP) X-Ray Powder Diffraction (XRPD) experiments were carried out at the BM01a beamline at ESRF (Grenoble-France) with a fixed wavelength of 0.6974 Å using a modified Merril-Bassett Diamond Anvil Cell (DAC).[10] The adopted pressure transmitting medium (PTM) was a mixture of ethanol:water (e.w.) characterized by a 1:3 composition ratio. This choice of PTM, suggested by previous experimental work [9a] and other literature studies,[11] was aimed at inserting both water and alcohol molecules in the zeolite framework. Because only water was incorporated in Si-FER using the aqueous penetrating PTM normally adopted in high-pressure studies on zeolites - a mixture of methanol : ethanol : water (m.e.w.) in ratio 16:3:1 –,[9a] here we considered a medium of composition different from that of the standard m.e.w. Specifically, we opted for a binary ethanol and water mixture characterized by a higher proportion of water with respect to m.e.w. in order to have water as dominant component of the mixture. The ratio e:w= 1:3 was selected on the basis of the results reported by Likhacheva et al (2007).[11] These authors observed no pressure-induced hydration (PHI) of the zeolite thomsonite with m.e.w., but they were able to achieve PHI by using a high concentration of water (> 50%) in the pressure medium..

These results suggested us that a similar change in the composition of the pressure transmitting medium might probably affect also the nature of the species incorporated in Si-FER at high pressures.

Pressure (P) was calibrated using the ruby fluorescence method[12] on the non-linear hydrostatic pressure scale.[13] The estimated precision of the P values is 0.05 GPa. The experiments were performed in the 0.2 - 1.34 GPa range; at higher pressures, ice formation occurred.

To test the reversibility of the process, some patterns were collected upon decompression, from the highest pressure in the explored range (1.34 GPa) to ambient pressure (Pamb). In this respect, the pressure was fully released by opening the DAC (the apparatus was a screw-based cell) and the Ruby fluorescence was measured at ambient pressure. The diffraction data were collected in the Debye–Scherrer geometry on Pilatus IP detectors (with pixel dimensions of 172 µm x 172 µm, respectively) at a fixed distance of 230 mm. One-dimensional diffraction patterns were obtained by integrating the two dimensional images with the program FIT2D.[14] Rietveld profile fitting was performed using the GSAS package[14b] with the EXPGUI[15] interface. Integrated patterns at selected pressures are reported in Figure 1 of the main text.

The unit cell parameters were determined by Rietveld profile fitting throughout the investigated pressure range. The refined cell parameters are reported in Table S1 and Figure 2 of the main text. The occurrence of new peaks at 1.04 GPa is due to a phase transition from the original orthorhombic space group of ferrierite (*Pmnn*), to the monoclinic space group ($P2_1/n$) (see Figure 1b of the main text).

e.w.					
	***a* (Å)**	***b* (Å)**	***c* (Å)**	***V* (Å^3)**	**β (°)**
P_{amb}	18.708(1)	14.0690(8)	7.4177(4)	1952.4(2)	
0.40	18.664(3)	14.019(1)	7.3835(7)	1932.0(5)	
0.67	18.628(3)	13.989(1)	7.3687(7)	1920.2(5)	
0.84	18.588(3)	13.966(1)	7.3596(7)	1910.5(5)	
1.04	18.579(8)	13.939(4)	7.357(2)	1905(1)	90.0(1)
1.34	18.553(5)	13.874(4)	7.353(2)	1892.8(8)	89.9(1)
0.68 (rev)	18.635(3)	13.987(1)	7.3677(8)	1920.4(5)	
P_{amb} (rev)	18.769(2)	14.074(1)	7.4234(6)	1961.2(5)	

Table S1. Unit-cell parameters of Si-FER compressed in ethanol:water (1:3) at the investigated pressures.

The structural refinement was performed at 0.84 GPa. The starting atomic coordinates of the framework for the refinement of the orthorhombic and monoclinic phases were based on the structural models of Refs. 9a and 9b, respectively. Due to the high thermal displacement (probably originating from statistical disorder in the structure), atom O5 was split in two positions whose occupancy sum was forced to be equal to 1. The positions of the intruded molecules were deduced from the inspection of the Fourier difference maps. The background curve was fitted by a Chebyshew polynomial with 20 coefficients. The pseudo-Voigt profile function proposed in Ref. 16 was applied, and the peak intensity cut-off was set to 0.1% of the peak maximum. Soft-restraints were applied to the T-O distances [Si-O = 1.58(2)-1.62(3)] C-C=1.52(2) and C-O =1.45(3). The isotropic displacement parameters were constrained as follows: the same value for all the tetrahedral cations, the same value for all the framework oxygen atoms, the same value for the ethanol molecule atoms and, finally, the same value for the water molecules. The isotropic thermal parameters of the extra framework species were refined once and then kept fixed to avoid correlations with other variables. The unit-cell parameters were allowed to vary in all the refinement cycles.

The structure of Si-FER obtained from the refinement of the powder data collected at 0.84 GPa is shown in Figure S1, the atomic coordinates and selected interatomic distances are reported in Tables S2 and S3. The values in Table S3 indicate that, although the model obtained from the refinement provides a reliable representation of the Si-FER framework, it is unfortunately characterized by too-short interatomic separations between the extraframework species (highlighted in red in Table S3). Actually, it is well known that the determination of light guest molecules in the cavities of porous materials by structural refinement is extremely challenging, being their localization from electronic density maps very problematic.[17] For these reasons, the refined data - giving about 6-8 H_2O and 4 ethanol molecules in the channels - were used as a starting point for determining the structure of the Si-FER/EtOH/H_2O system via density functional calculations.

Table S2. Refined coordinates, occupancy factors and isotropic thermal parameter for Si-FER at 0.84 GPa.

	x/a	y/b	z/c	Occ	Uiso
Si1	0.148(1)	0	0	1	0.019(3)
Si2	0.277(1)	-0.003(2)	0.285(1)	1	0.019(3)
Si3	0.0761(7)	0.195(1)	-0.002(5)	1	0.019(3)
Si4	0.339(1)	0.193(2)	0.212(5)	1	0.019(3)
Si5	0.685(2)	0.780(2)	0.208(5)	1	0.019(3)
O1	0.262(3)	0	0.5	1	0.027(6)
O2	0.204(1)	-0.002(9)	0.165(5)	1	0.027(6)
O3	0.088(2)	0.082(2)	0.007(15)	1	0.027(6)
O4	0.650(2)	0.783(3)	-0.001(4)	1	0.027(6)
O5	0	0.238(2)	0.057(6)	0.9	0.027(6)
O5b	0.5	0.272(2)	0.55(3)	0.1	0.027(6)
O6	0.264(3)	0.243(6)	0.25(1)	1	0.027(6)
O7	0.123(3)	0.241(4)	0.164(5)	1	0.027(6)
O8	0.901(2)	0.737(4)	0.168(5)	1	0.027(6)
O9	0.334(2)	0.0811(19)	0.253(7)	1	0.027(6)
O10	0.694(3)	0.8928(24)	0.240(9)	1	0.027(6)
OH1	0.476(21)	0.926(18)	0.253(15)	0.25	0.14
C11	0.45(2)	0.93(1)	0.44(1)	0.25	0.14
C12	0.49(1)	1.02(2)	0.502(9)	0.25	0.14
OH2	0.53(1)	-0.03(1)	0.86(2)	0.25	0.14
C21	0.54(2)	0.02(2)	1.04(1)	0.25	0.14
C22	0.51(2)	0.10(2)	0.895(9)	0.25	0.14
W1	0	-0.33(2)	0.35(2)	0.54(9)	0.18
W2	0	0	0.5	0.9(1)	0.18
W4	0	0.14(1)	0.52(2)	0.92(8)	0.18

Table S3. Experimental interatomic distances (shorter than 3.2 Å) for Si-FER at 0.84 GPa.

		distance (Å)	
Si1-	O2	1.602(2)	
	O2	1.602(2)	
	O3	1.602(2)	
	O3	1.602(2)	
Si2-	O1	1.608(3)	
	O2	1.606(3)	
	O9	1.607(3)	
	O10	1.586(3)	
Si3-	O3	1.603(3)	
	O5	1.596(3)	
	O7	1.626(3)	
	O8	1.605(3)	
	O5b	1.524(1)	
Si4-	O4	1.586(3)	
	O6	1.587(3)	
	O8	1.585(3)	
	O9	1.587(3)	
Si5-	O4	1.607(3)	
	O6	1.587(3)	
	O7	1.587(3)	
	O10	1.606(3)	
OH1-	O9	2.9290(6)	
	O10	3.1366(8)	
	C11	1.50061(27)	
	C21	2.54143(31)	
	W1	3.11(26)	
	OH2	2.8041(4)	
C11-	O5	2.8204(5)	
	O8	3.1587(4)	
	OH1	1.50061(27)	x2
	C12	1.52058(22)	x2

		distance (Å)	
C12-	C11	1.52058(22)	x2
	OH2	3.0360(5)	x2
	C22	2.7695(4)	
OH2-	O9	2.6324(6)	
	OH1	2.8041(4)	
	C11	3.1354(4)	
	C12	3.0360(5)	
	C21	1.50844(22)	
	W1	**2.07(24)**	
C21-	O9	3.1517(6)	
	OH1	2.54143(31)	
	OH2	1.50844(22)	
	C22	1.51731(21)	
C22-	O5	2.7996(4)	
	C12	2.7695(4)	
	C21	1.51731(21)	
W1-	**O8**	**2.46(11)**	
	OH1	3.11(26)	
	W4	2.71(21)	
W2-	**W4**	**2.10(21)**	
W4-	O8	3.04(16)	
	W1	2.71(21)	
	W2	**2.10(21)**	

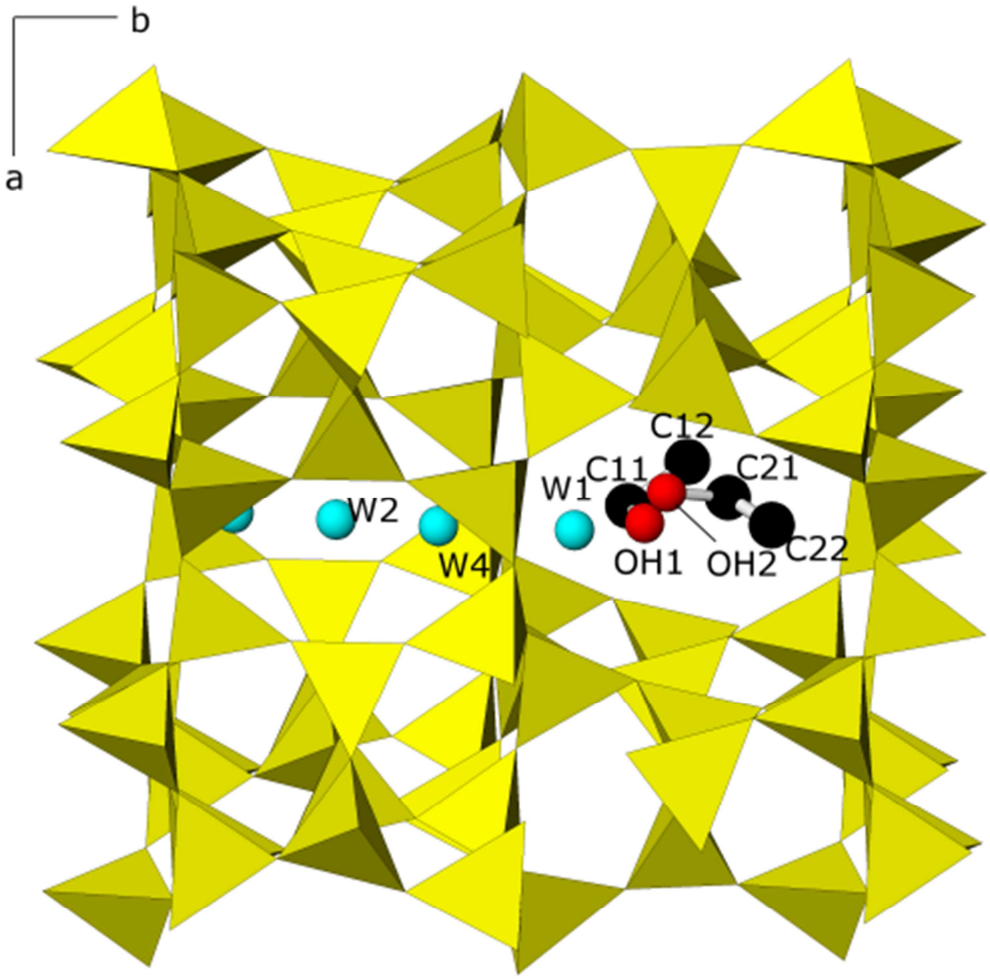

Figure S1. Graphical representation of the structure obtained from the refinement of the powder data collected for Si-FER compressed in e.w. (1:3) at 0.84 GPa. Atom labels as in Table S2. Atom colors: Si tetrahedra: yellow; O (water): cyan; EtOH oxygen positions (OH1, OH2): red, EtOH carbon position (C11, C12, C21, C22):black.

2. COMPUTATIONAL METHODS AND MODELS

Water-ethanol mixtures confined inside the Si-FER framework at GPa pressure regimes were investigated by a Density Functional Theory (DFT) approach,[18] with plane waves (PW) as basis set and periodic boundary conditions in 3-dimensions.[19] The simulation cell, characterized by a framework stoichiometry of [$Si_{72}O_{144}$], was generated by adopting the unit cell parameters experimentally determined for Si-FER at 0.84 GPa (namely: *a*=18.588 Å; *b*=13.966 Å; *c*= 7.3596 Å, see also Table S1) and replicating 2 unit cells along the *c*-axis. Hence, the adopted simulation cell parameters were: *a*=18.588 Å; *b*=13.966 Å; *c*= 14.7192 Å. As mentioned in the previous section, the extraframework content of the simulation systems was defined with the aid of the experimental data obtained at 0.84 GPa, which suggested the intrusion of 4 ethanol molecules and about 6-8 water molecules *per* Si-FER unit cell. Therefore, the first and fundamental problem that modeling had to solve was to determine the exact number of water molecules encapsulated in Si-FER at 0.84 GPa. To this aim, we kept the cell parameters fixed at their experimentally determined values – that are well known to be accurate[17] – and varied the water content (i.e. the number of water molecules, *n*) in the simulation cell. For each water content *n*, all atomic positions were then optimized, without imposing any symmetry constraints. To determine the cell stoichiometry, we searched for the water content that minimized the total energy.

More specifically, to sample a sufficiently broad set of situations where 4 ethanol (EtOH) molecules and *n* water molecules *per* crystallographic unit cell were present, we built six simulation systems characterized by a general stoichiometry of [$Si_{72}O_{144}$]·8EtOH·*n*H_2O (FER·8EtOH·*n*H_2O) with *n*=12,14,16,20,24,28. We then studied their relative stability by performing DFT-based structural optimizations.

To search for energy minima, the atomic positions of all atoms of the adopted models were optimized, while the cell parameters were held fixed at the experimental values. The Perdew-Burke-Ernzenhof (PBE) approximation to DFT[18a] was adopted throughout for the electronic structure treatment, in conjunction with the Grimme corrections[18b] for dispersion. In this theoretical scheme, an empirical correction term for long-range dispersion effects is added to the PBE functional; such a correction is defined as a combination of damped interatomic potentials of C_6R^{-6} form.[18b] It is worth mentioning that a detailed analysis of the agreement between DFT-optimized structures and experimental crystal structures has been recently performed for a broad set of neutral-framework zeolites by using several generalized-gradient-approximation (GGA) functionals (also including dispersion corrections).[20a] The DFT results were also compared with data obtained with the dispersion-corrected hybrid functional B3LYP and with molecular-mechanics force fields.[20a] Such a benchmark study showed that the inclusion of a dispersion correction greatly improves the performances of the GGA functionals in predicting zeolite structural parameters, and

suggested the dispersion-corrected PBE functional as a reasonable default choice for structural optimizations of zeolites characterized by a neutral framework. Also importantly, a similar systematic benchmark investigation on water-containing aluminosilicate zeolites noted that in DFT-predictions of zeolite structures it is often preferred to fix the lattice parameters to accurate experimental values (where available); such study concluded that, among the tested DFT-approximations, the dispersion-corrected PBE functional was the one providing the best performances in terms of the agreement between DFT and experimental structural data.[20b] On these bases, we consider the DFT-approximations adopted in this study to be appropriate for modeling the behavior of water and ethanol in Si-FER.

Because of the sufficiently large values of the simulation cell parameters, only the Γ point of the Brillouin zone was considered in all of the calculations. The electron-nuclei interactions were described via pseudopotentials. Ultra-soft pseudopotentials were used for O, C, H atoms,[21] while norm-conserving pseudopotentials were adopted for Si.[22-24] Electronic states were expanded in PW up to a cutoff of 25 Ry, while the electronic density was expanded up to 200 Ry.

Calculations were performed with the CPMD code.[19] Specifically, the geometry optimizations were performed via a quasi-Newton approach and stopped when maximum forces on the nuclear positions were below 5×10^{-4} hartree/bohr. For each system, a few-picosecond-long first principles molecular dynamics (FPMD)[25] equilibration run was carried out at room temperature before the geometry optimization. In these equilibration simulations, we used the same computational set-up of the geometry optimizations. The integration time step was 0.121 fs and a fictitious inertia parameter of 500 au was used for the electronic part of the Car-Parrinello equations. In all of the calculations performed for this study, all atoms were allowed to move, no symmetry constraint (except from the box shape and size) was imposed, and periodic boundary conditions were applied.

The stabilization energies for the FER·8EtOH·$n$$H_2O$ systems with respect to the isolated components (i.e. the zeolite framework and the guest molecules) were calculated by using Equation 1:

$$\Delta E(\text{FER}\cdot 8\text{EtOH}\cdot n\text{H}_2\text{O}) = E(\text{FER}\cdot 8E\text{tOH}\cdot n\text{H}_2\text{O}) - E(\text{FER}) - 8\times E(\text{EtOH}) - n\times E(\text{H}_2\text{O}) \quad (1)$$

where E(FER·8EtOH·$n$$H_2O$) is the energy of the optimized structure (with n = 12,14,16,20,24,28), E(FER) is the energy of the empty all-silica FER zeolite model, while E(EtOH) and E(H_2O) are the energies of an isolated EtOH molecule and an isolated H_2O molecule, respectively, calculated in the same simulation cell. In the case of isolated EtOH, both the trans (t) and gauche (g) conformers[26] were considered, resulting however in nearly isoenergetic structures (ΔE(g-t) = 0.01 kcal/mol), in line with previous studies.[26] In this respect, we point out that the arrangement of the ethanol molecules in the optimized geometries of the FER·8EtOH·$n$$H_2O$ models always features

rows of ethanol dimers aligned along the 10-MR channel axis (see Figure 3b of the main text). The dominant configuration of the ethanol dimers corresponds to a structure with both monomers in the gauche conformation, in agreement with recent reports (see e.g. Ref. 26c and references therein) However, in the case of the ethanol dimer the energy differences among different conformers are often too small to be discerned by experimental or theoretical methods.[26]

The relative stabilities of the models were calculated with respect to the model with the lowest water content (12 water molecules *per* simulation cell, corresponding to 6 water molecules *per* crystallographic unit cell). For example, in the case of the system with 14 water molecules:

$$\Delta E(12/14) = E(\text{FER}\bullet 8\text{EtOH}\bullet 14\text{H}_2\text{O}) - [E(\text{FER}\bullet 8\text{EtOH}\bullet 12\text{H}_2\text{O}) - 2\times E(\text{H}_2\text{O})] \qquad (2)$$

The values of the relative stabilities reported in this work (e.g., in Figure 3a of the main text) are given in kcal *per* mol of crystallographic unit cell, which corresponds to half of the simulation cell. The general stoichiometry of the crystallographic unit cell for the models considered in this study is $[Si_{36}O_{72}]\cdot 4EtOH\cdot n H_2O$ (Si-FER·4EtOH·nH$_2$O), with n=6,7,8,10,12,14. The system containing 8 water molecules *per* crystallographic unit cell was found to be the most stable one. To explore the behavior of this system (namely, Si-FER·4EtOH·8H$_2$O) at room temperature conditions – and, especially, the stability of the supramolecular organization of the extraframework species - a FPMD simulation was performed, starting from the corresponding minimum energy structure. The simulation was carried out at 300 K with the same computational set-up of the short FPMD runs preliminary to optimization (Nose thermostats[27] on the ionic degrees of freedom, integration time step = 0.121 fs and fictitious inertia parameter = 500 au). After 5 ps thermalization and equilibration, production data were collected on a 12 ps long trajectory. As mentioned in the main text and referenced therein, such an approach for electronic structure treatment, geometry optimization and molecular dynamics has provided a reliable description of complex organic-inorganic systems in a broad variety of situations, from room conditions to high temperature/high pressure conditions. In particular, this scheme has been successfully employed in a recent combined experimental–computational study on the high-pressure behavior of the fibrous zeolite $Rb_7NaGa_8Si_{12}O_{40}\cdot 3H_2O$ with the edingtonite (EDI) topology.[17c] As a further, '*a-posteriori*', check of the validity of this approach, we compared the positions of the Si-FER framework atoms obtained from the FPMD production run with the corresponding experimental values from the refinement of the X-ray data at 0.84 GPa. The FPMD-predicted positions of the framework atoms compared satisfactorily with the experimental ones (see Figure S2, in section 3). The largest deviations affect the T-O-T angles: this was however expected on the basis of the known tendency of dispersion-corrected DFT functionals to underestimate these angles.[20a] This comparison further supports the validity of the adopted theoretical approach in the description of the high-pressure behavior of Si-FER. Selected structural results from the FPMD production run are also reported in Section 3 (Table S4, Figures S3-S4, Discussion of the FPMD simulation results).

Finally, to investigate the behavior of the system upon decompression, and, specifically, whether the pressure-induced inclusion of water and ethanol was irreversible, we built three new models (containing 4 EtOH and *n*= 7, 8 and 10 water molecules per crystallographic unit cell, respectively), characterized by the cell parameters experimentally determined at ambient conditions after pressure release, namely: *a* = 18.769 Å; *b* = 14.074 Å; *c* = 2 × 7.4234 Å (see also entry P_{amb}(rev) in Table 1 of the main text, and in Table S4). The optimized atomic positions calculated for the models corresponding to the cell parameters at *P*=0.84 GPa were taken as starting coordinates for this new set of structural optimizations, which were performed by adopting the same computational setup as above described. Before geometry optimization, an equilibration FPMD run was performed at T=300 K (using the setup previously described for the other FPMD simulations) in order to allow for the atomic positions to properly relax to the cell parameters determined after pressure release, i.e., at P_{amb} (rev).

The geometry optimizations of the three above-mentioned models of the Si-FER system in the decompression regime, and the calculations of their stabilization energies using Eq. 1-2, provided the following results:

- all three systems (namely, Si-FER·4EtOH·*n*H_2O, with *n*=7,8,10) are more stable than the separated components also at P_{amb}(rev), confirming the experimental evidence of no leaking of extraframework species upon pressure release.
- Their stabilization energies slightly increase upon pressure release with respect to the corresponding values obtained for 0.84 GPa conditions. For the systems containing *n* = 7,8,10 H_2O *per* crystallographic unit cell, this increase amounts to 1.3, 1.2 and 6.9 kcal/mol, respectively.
- The relative stability order of the three systems remains unaltered with respect to that found at 0.84 GPa conditions: namely, the Si-FER model containing 8H_2O *per* crystallographic unit cell is the most stable one also upon pressure release.

On the whole, the results of this new series of calculations indicate that the formation of the 2D network of alternating water / ethanol supramolecular subunits in ferrierite, accomplished via the application of an external pressure, is irreversible: the organization is remarkably stable, and is fully maintained upon complete pressure release.

Furthermore, the behavior of the most stable model Si-FER·4EtOH·8H_2O (8 water molecules *per* crystallographic unit cell) was studied at room temperature conditions by performing a FPMD simulation starting from the optimized geometry. After 5 ps thermalization and equilibration, production data were collected on a 12 ps long trajectory. Selected results of this simulation on the decompressed system are also discussed in Section 3. (Table S4, Figures S3-S4, Discussion of the FPMD results).

Finally, concerning the calculated minimum energy structures, two pdb files containing the xyz-coordinates for the atoms in the simulation cell are also provided, named W8_084_GPa_min.pdb and W8_Pamb_Rev_min.pdb. They refer to the optimized structures of Si-FER•4EtOH•8H_2O corresponding to *P*=0.84 GPa and P_{amb}(rev), respectively.

3. ADDITIONAL COMPUTATIONAL RESULTS

3.1. Results of First Principles Molecular Dynamics simulations: Table S4, Figures S2-S4

Table S4. Hydrogen bond distances (Å) for EtOH dimers and water tetramers in Si-FER·4EtOH·8H_2O calculated from the FPMD simulations relative to 0.84 GPa and P_{amb}(rev)

[a]EtOH	(i)		(ii)	
[b]	0.84 GPa	P_{amb}(rev)	0.84 GPa	P_{amb}(rev)
O_{E1}-H_{E2}	1.956 (0.296)	1.922 (0.217)	1.831 (0.136)	1.933 (0.228)
[a]H_2O tetram.	(i)		(ii)	
[c]	0.84 GPa	P_{amb}(rev)	0.84 GPa	P_{amb}(rev)
O_{W1}-H_{W2}	1.796 (0.161)	1.791 (0.161)	1.891 (0.274)	1.850 (0.186)
O_{W2}-H_{W3}	1.740 (0.138)	1.807 (0.175)	1.845 (0.168)	1.843 (0.174)
O_{W3}-H_{W4}	1.770 (0.160)	1.780 (0.137)	1.719 (0.137)	1.754 (0.145)
O_{W4}-H_{W1}	1.780 (0.173)	1.806 (0.174)	1.702 (0.134)	1.746 (0.152)

[a](i), (ii): the two distinct EtOH dimers/water tetramers in the Si-FER unit cell. [b]E1 and E2: the two EtOH's in each dimer. [c]W1,2,3,4: the four H_2O's in each tetramer. All the reported hydrogen-bond distances are averaged first over the simulation length (12 ps) and then over the simulation cell (containing 2 crystallographic unit cells). Standard deviations (in parentheses) provide an estimate of the average thermal fluctuations of the hydrogen-bonding distances.

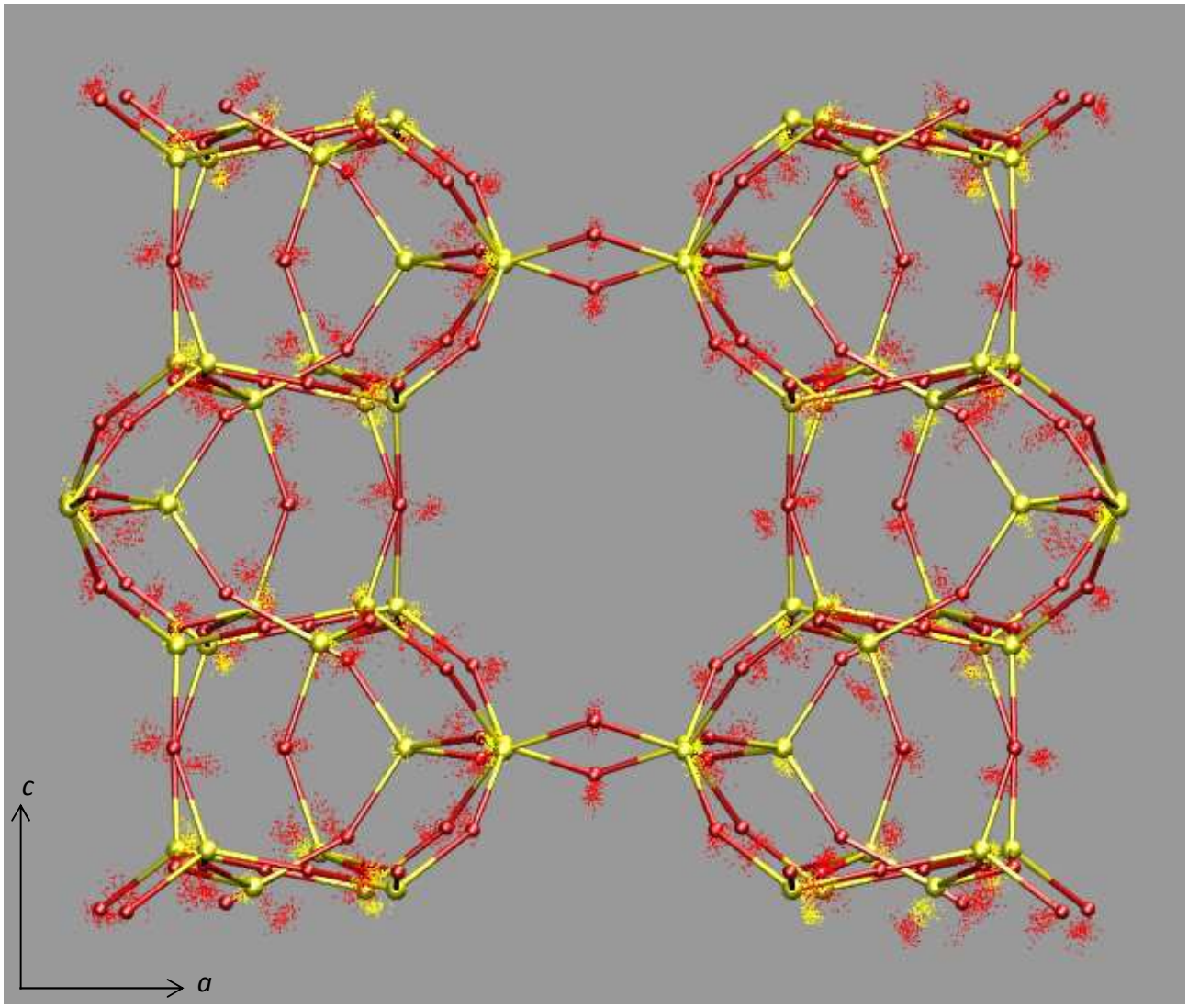

Figure S2. Comparison between the positions of the Si-FER framework atoms obtained from the refinement of the X-ray data collected at 0.84 GPa (ball-and-stick representation) and the corresponding atomic positions sampled at 10 fs intervals along the FPMD simulation (dots representation). Atom color codes: Si=yellow; O=red.

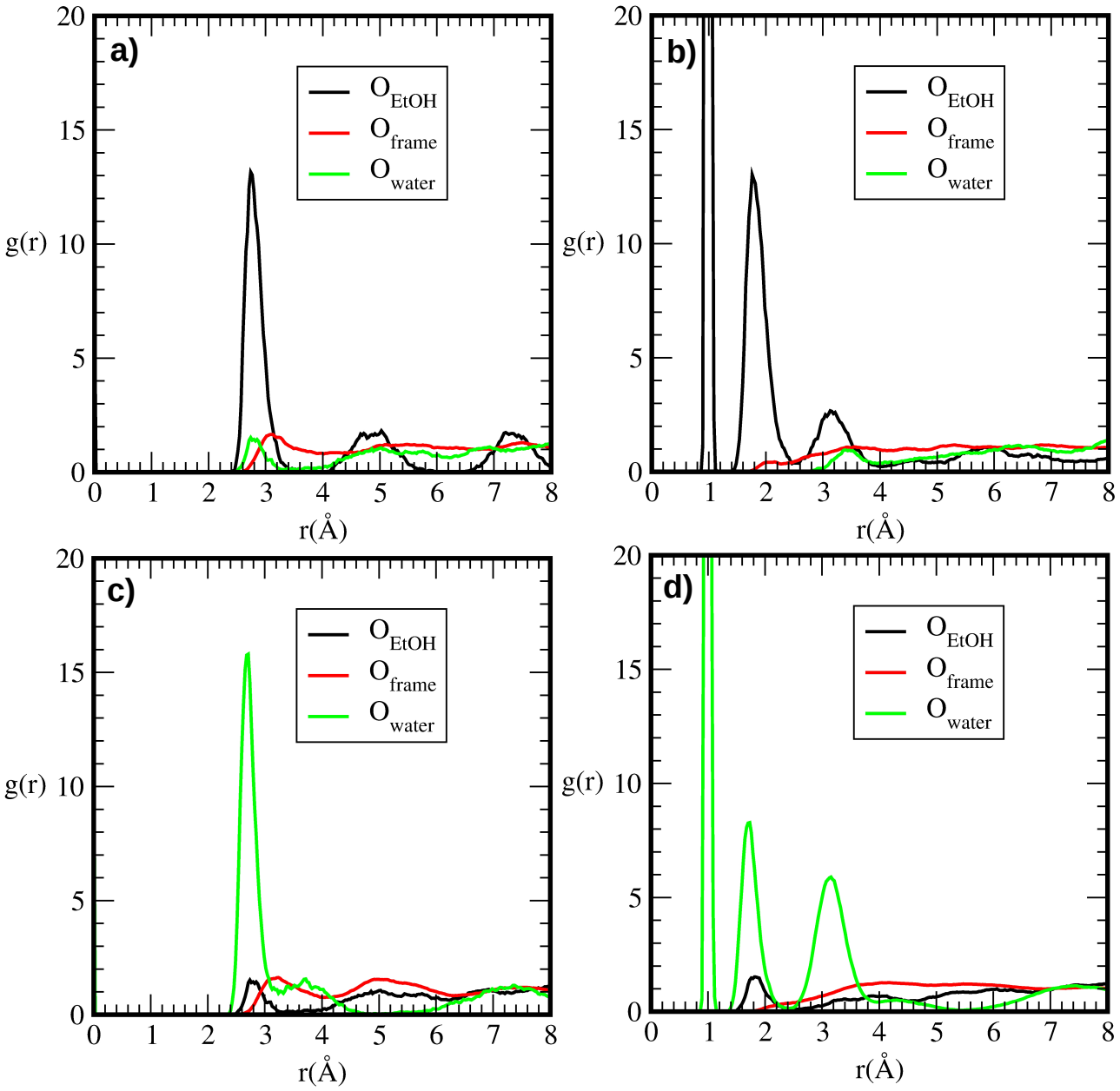

Figure S3. Pair distribution functions g(r) obtained from the room-temperature FPMD simulation of Si-FER·4EtOH·8H_2O relative to *P*=0.84 GPa. The reported g(r)'s are relative to: EtOH oxygen atoms, panel a; EtOH hydroxyl protons, panel b; water oxygen atoms, panel c; water protons, panel d.

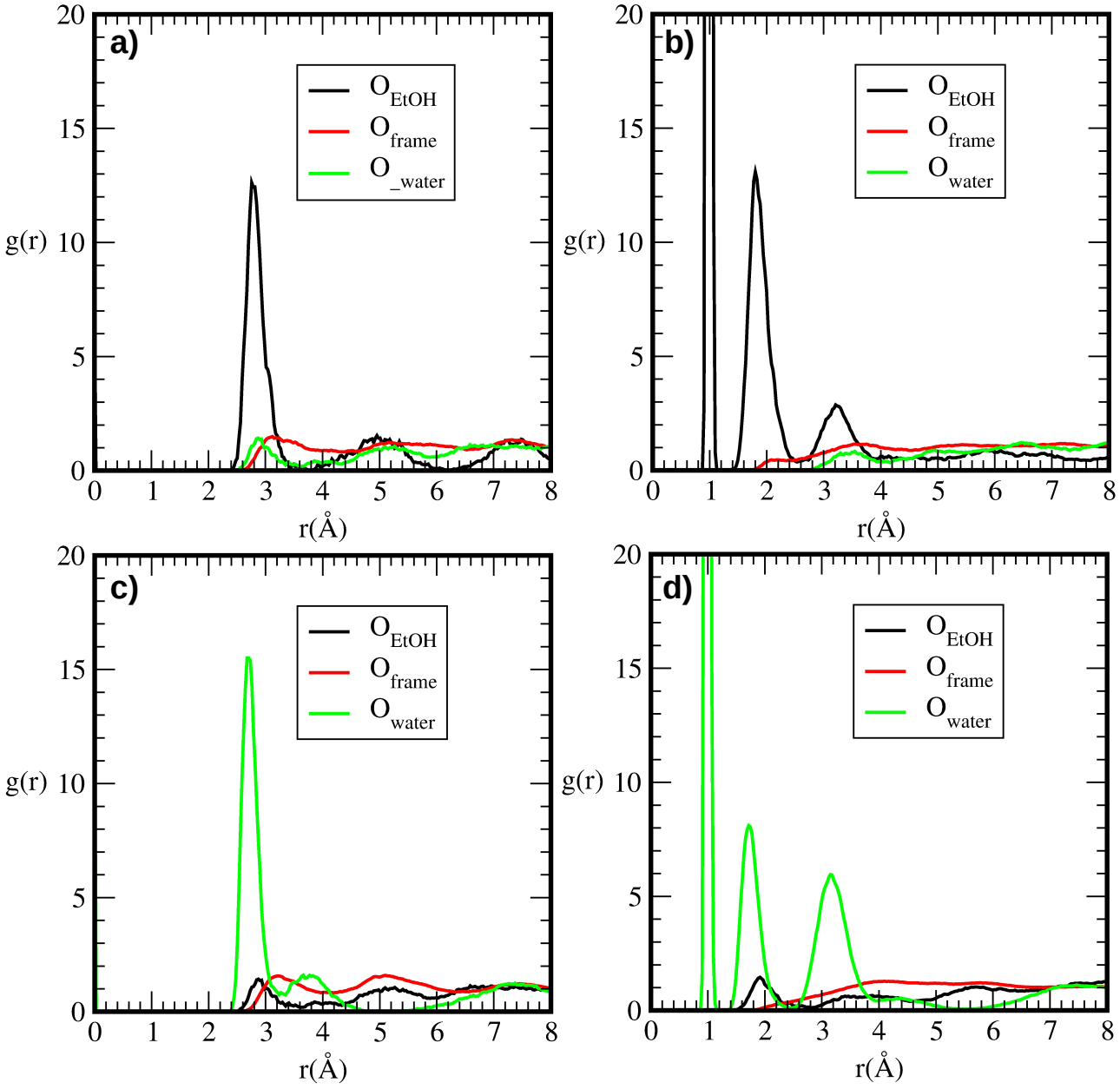

Figure S4. Pair distribution functions g(r) obtained from the room-temperature FPMD simulation of Si-FER·4EtOH·8H_2O relative to *P*=P_{amb} (rev) (release to room pressure conditions). The reported g(r)'s are relative to: EtOH oxygen atoms, panel a; EtOH hydroxyl protons, panel b; water oxygen atoms, panel c; water protons, panel d.

3.2. Discussion of the results of First Principles Molecular Dynamics simulations

Important insight on the behavior of guest molecules inside the zeolite pores may be gathered from pair distribution functions (a.k.a. pair correlation functions, or radial distribution functions) g(r), which provide information on the average separation between guest species, or between guest species and the zeolite framework walls. For example, the pair correlation functions among hydrogen and oxygen atoms can evidence the presence of stable hydrogen bonds at room temperature conditions.

First, we consider the g(r) calculated for the Si-FER·4EtOH·8H_2O system for high pressure conditions (0.84 GPa), reported in Figure S3. It is worth stressing that the g(r) related to the separation between the oxygen atoms of two ethanol molecules (Figure S3, a) has a very strong peak at 2.74 Å, which clearly indicates the presence of strong hydrogen bonds between ethanol molecules. Such hydrogen bonds are those of the ethanol dimers. The peaks in the 2.73-3.10 Å region of the g(r)'s, pertaining to the O_{EtOH}-O_{water} and O_{EtOH}-$O_{framework}$ distances, are much weaker, indicating therefore that interactions of the ethanol molecules with both framework and water oxygen atoms play only a minor role. The g(r)'s corresponding to the EtOH hydroxyl protons (Figure S3, b), apart from the peak of the intramolecular bonds with the EtOH oxygens (0.99 Å), are characterized by a strong intermolecular peak at 1.76 Å, which is the signature of hydrogen bonding with the nearest EtOH molecule. We also observe a peak, with very low intensity, at about 2.1 Å in the g(r) with the framework oxygens, indicating a weak interaction of ethanol with the Si-FER oxygen atoms as well. No relevant interaction among ethanol hydroxyl protons and water oxygen is detected.

By considering now water molecules, the g(r) corresponding to the water oxygen atoms (Figure S3, c) evidences a very strong water-water interaction with a high-intensity peak at 2.69 Å. A weaker interaction with EtOH oxygens is also present, as highlighted by the corresponding g(r), which shows a low-intensity peak at 2.82 Å (Figure S3, c). Moreover, the water oxygen-framework oxygen pair distribution, with its weak peak at 3.2 Å, indicates that water-framework interactions are only weak and labile. Last, the radial distributions of H_2O protons, depicted in Figure S3, d), is characterized by the peak of the O-H intramolecular bond at 1.0 Å and by a very strong, neat peak at 1.72 Å, corresponding to the water-water interaction. Altogether, these features indicate: (i) strong water-water hydrogen bonds; (ii) the presence of some hydrogen bonds between water protons and EtOH oxygen atoms (as evidenced by the weaker peak at 1.82 Å) and (iii) no relevant short-range interactions with framework oxygen atoms.

By performing now the same analysis on the g(r)'s calculated from the trajectory corresponding to the released pressure regime (P_{amb}(rev)), a striking similarity emerges with the results obtained for the high-pressure regime. Indeed, comparison between Figures S3 and S4 is clear evidence that the release of external pressure brings about no significant change to the organization of water and ethanol in Si-FER realized at high pressure conditions.

These findings are also confirmed by the average values of the hydrogen-bond distances relative to the extraframework species, calculated from the two FPMD simulations and reported in table S4.

On the whole, this analysis of the behavior of the Si-FER·4EtOH·8H_2O system, performed on the two FPMD trajectories at room temperature conditions, highlights a remarkable stability of the pressure-induced water-ethanol supramolecular organization in Si-FER, and strengthens the

conclusions emerged from the analysis of the minimum energy structures – namely, that the water and the organic subsystems occupy different domains of the porous host, and that this peculiar segregation into a two-dimensional binary architecture of supramolecular components is irreversible upon decompression.

3.3 Graphical representation of the water clusters in Si-FER

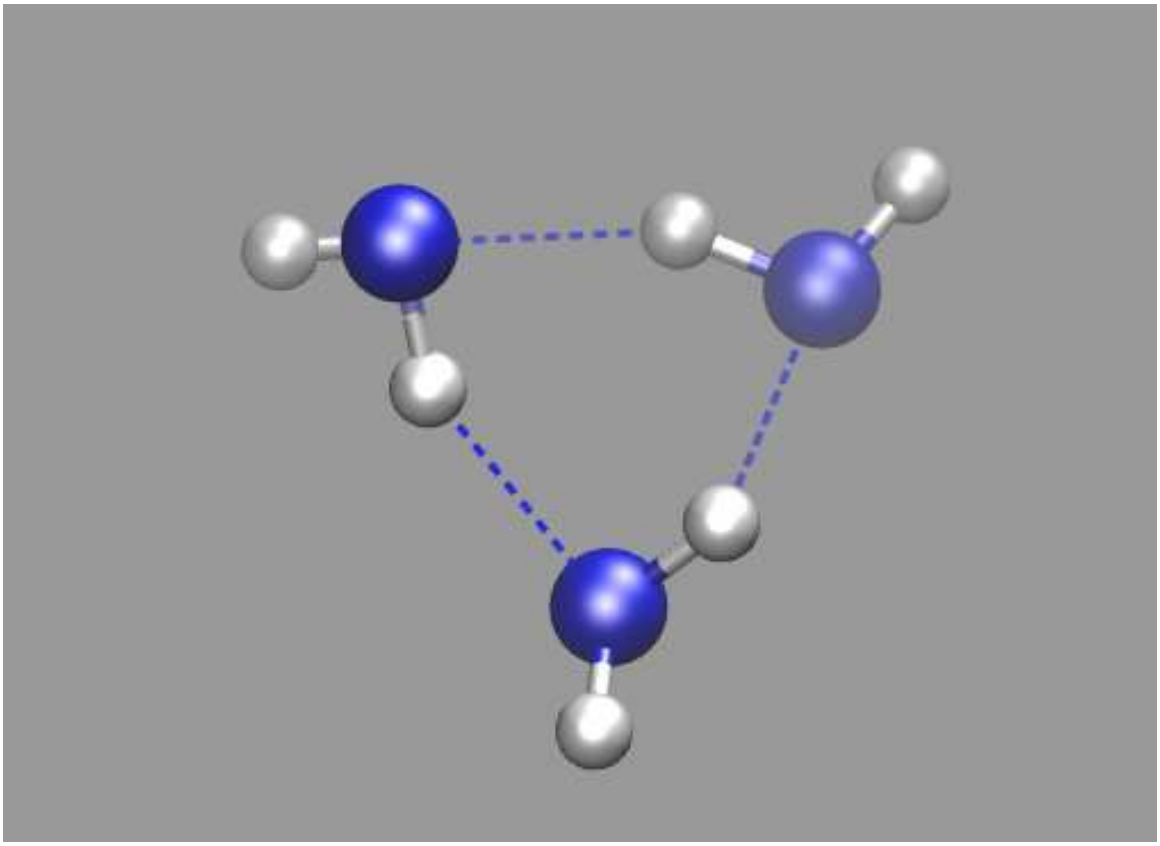

Figure S5. Graphical representation of the water trimers in the Si-FER·4EtOH·6H_2O system. Color codes: O=blue; H= white. Blue dashed lines indicate hydrogen bonds.

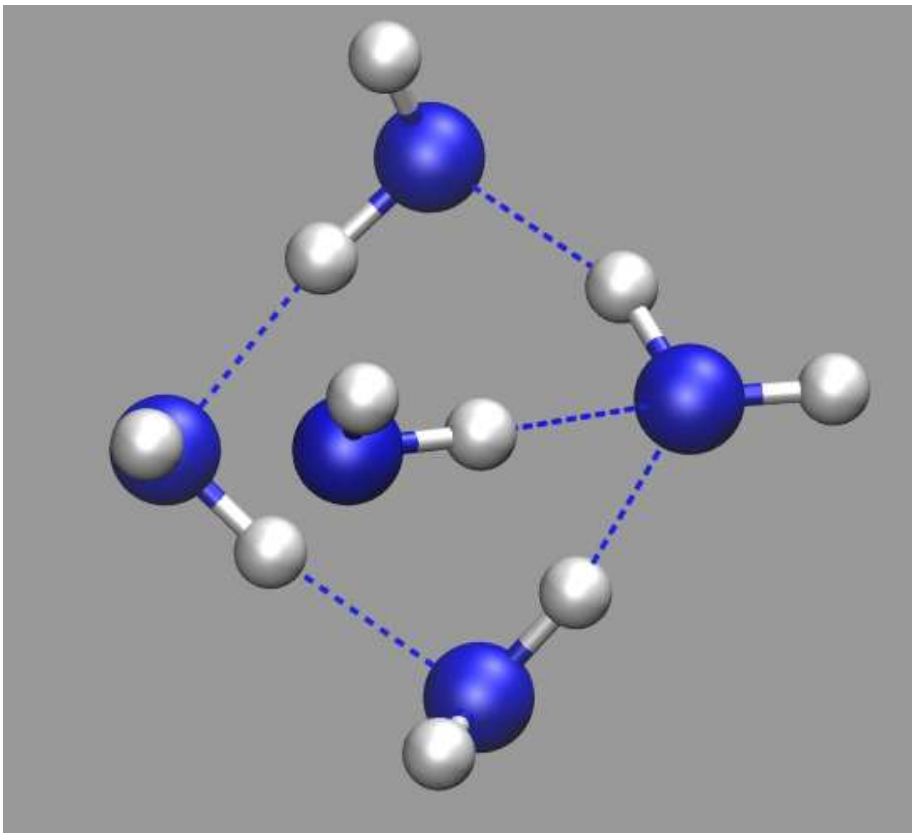

Figure S6. The water pentamers in the Si-FER·4EtOH·10H_2O system. Color codes as in figure S5.

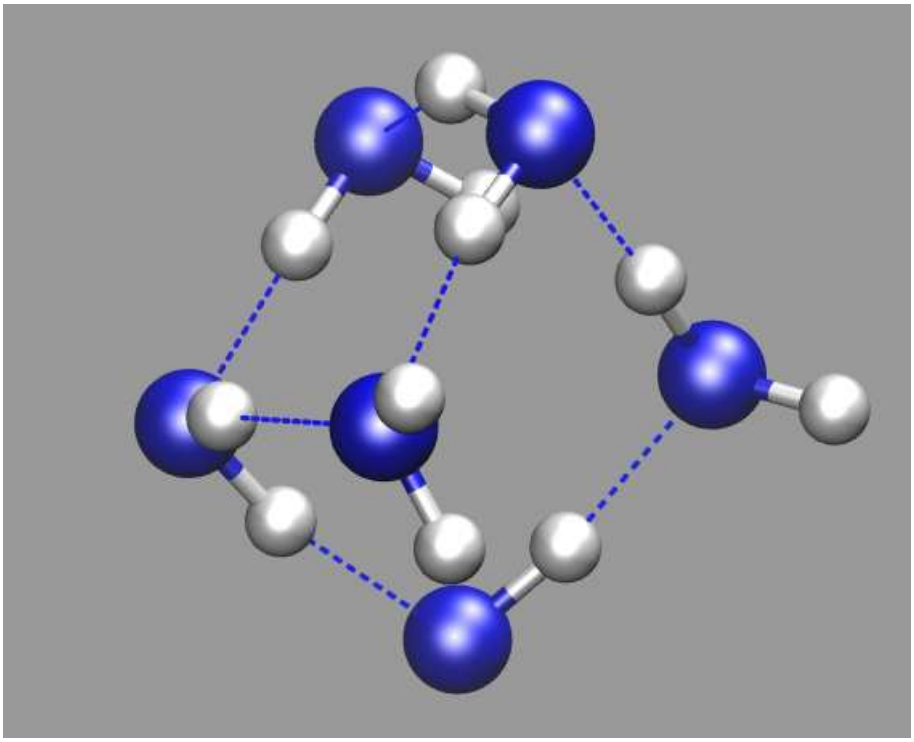

Figure S7. The water hexamers in the Si-FER·4EtOH·12H_2O system. Color codes as in figure S5.

4. GENERAL DISCUSSION ON OUR FINDINGS, OPEN QUESTIONS, AND PERSPECTIVES

4.1 Role of the maximum applied pressure and of the pressure medium

More light could be shed on our findings by comparing them with other intrusion experiments of molecular species in hydrophobic zeolite frameworks. In particular, besides the high-pressure study of Arletti et al. (Ref. 9a), condensation of water in the hydrophobic framework of Si-FER was also investigated by Cailliez et al (Ref. 28). These authors report a pure water intrusion-extrusion experiment, which was performed using an intrusion-extrusion porosimeter. Notably, complete filling of the Si-FER framework was obtained, although the highest pressure reached in such experiment was 0.30 GPa only. Specifically, water intrusion was observed around 0.15 GPa, and was followed by a plateau - indicating full loading of the host – at about 14 molecules/unit cell.[28] Remarkably, this result is in good agreement with our findings (full loading of Si-FER with 8 H_2O and 4 EtOH per unit cell), if we consider that ethanol is somewhat bulkier than water. Furthermore, such a water content is also in line with that found at 0.2 GPa with m.e.w. using DAC (15 H_2O per unit cell)[9a] i.e., when only water was incorporated in Si-FER.[9a] This agreement leads to the hypothesis that: i) pressures below 0.3 GPa, i.e. significantly smaller than those adopted in our experiment, might be sufficient to achieve full loading of Si-FER with water and ethanol, ii) pressures above this onset should be responsible of the separation of water and ethanol and of the special arrangement found in our study.

Also very importantly, the most significant difference between our results and those by Cailliez et al., is that the pure water experiment reports a reversible intrusion-extrusion,[28] while in our high pressure ethanol-water experiments the clusters arrangement inside the pores remains stable upon pressure release. Note that irreversible uptake of water was also observed when Si-FER was loaded with m.e.w. – in such case, the maximum pressure reached with DAC was 1.5 GPa.[9a] This suggests that the difference between the behavior of our system (irreversible uptake of extraframework species) and that reported by Cailliez et al. (reversible intrusion-extrusion) should be reasonably due to the fact that the maximum applied pressure was considerably higher in our experiment. On this basis, we hypothesize that the irreversibility of both the loading and the segregation/organization processes should be induced by pressures higher than those needed to achieve complete filling of the zeolite framework. In this respect, a relevant question to be addressed is whether moderately high pressures (e.g., higher than 0.3 GPa, but lower than those reached in our experiment) might be sufficient to accomplish irreversible separation and organization at molecular level. As this would be highly desirable for practical applications, it would be particularly relevant to determine the pressure value at which the separation of the two components becomes appreciable and irreversible.

Clearly, much remains to be done to understand the relationships between the penetration and the organization process. For example, it would be interesting to establish whether the incorporated molecules suddenly form organized patterns above a certain pressure onset, or if rather the organization process begins with the intrusion and evolves gradually with increasing pressures. Related to this issue, is the role of the interface region, i.e. what happens when the molecules of the pressure transmitting medium come in contact with the zeolite pore openings. These problems arise because we have no knowledge about how the pressure-driven intrusion and organization processes take place at molecular level. Understanding the evolution of the framework loading and the organization of molecular content as a function of increasing pressure is one of the challenging issues to be addressed in future studies.

4.2 Role of the topology and chemical composition of the framework

As discussed in the main text of the manuscript, and more extensively here, in sections 1.2 and 4.1, the composition of the pressure transmitting medium and the value of the maximum applied pressure may have substantial effects on the process of pressure-induced molecular intrusion and organization. In this context, the influence of the framework topology and composition is also crucial.

The specific zeolite type – ferrierite - plays a fundamental role in determining the peculiar water-ethanol segregation in a two-dimensional arrangement. Ferrierite has two parallel channel systems of different dimensions – 6MR and 10MR - which are perfectly suited to accommodate small supramolecular units of the distinct individual components. In particular, a linear arrangement of ethanol dimers perfectly fits the 10MR channels, while water molecules can fill the 6MR ones forming clusters of very high stability. Additionally, the intersection space among the 6MR/10MR channels and the orthogonal 8MR ones is particularly small compared to other zeolite types, and the associated confinement effects are therefore strong enough to prevent a liquid-like condensation of mixed ethanol-water clusters.

The role of the chemical composition of the framework in pressure-induced organization/separation processes is another issue that needs to be investigated systematically. The question as to how the hydrophobic/hydrophilic character of the framework could affect such processes is of particular relevance, considering, e.g. the importance of Al-containing zeolites in innumerable applications. Although the present work – presenting the first evidence of a pressure-induced organized separation in zeolites – has been performed using a hydrophobic framework, previous studies provide useful indications that might help to predict what could be the behavior of intruded species in a hydrophilic zeolite.[29] Whereas in hydrophobic (all-silica) frameworks the intruded molecules interact only weakly with framework walls,[30] in Al-containing zeolites there could be strong and

specific interactions with both charge-balancing cations and zeolite framework walls (see Ref. 29 for a comprehensive review of high-pressure studies on hydrophilic zeolites). [29] A key role would be played by the nature of the charge-balancing cations, which can also influence the framework flexibility and consequently its deformations upon compression.[29,31] Overall, in hydrophilic frameworks the zeolite-molecule interactions would compete with intermolecular interactions in determining the organization of the intruded species. In some cases, such a competition might have detrimental effect on the supramolecular organization of confined species – especially at high pressure, when molecules are forced to be closer to the channel walls. [29] Indeed, some of the first high pressure experiments were performed on natural Al-rich zeolites that already contained well organized water structures. Notably, in a few cases, typically with small and highly polarizing cations like Li, the organization persisted at very high pressures as well, in spite of the presence of water-framework hydrogen bonds.[32] On this basis, we might hypothesize that moderately hydrophilic zeolites (i.e. with high Si/Al ratio), which have protons as extraframework cations (thus, Brønsted acid character) could probably still be adopted as containers to create, through application of moderately high pressures, ordered arrangements of molecular species. In this case, it should however be taken into account that the intruded species might also react with the Brønsted acid sites of the zeolite.

Addressing such questions might be particularly relevant, also in the perspective of applications in catalysis. Actually, zeolites are used not only in the separation steps but also in the actual production processes of biofuels - as catalysts. In such case, hydrophilic zeolites – containing acid sites – are needed to perform the cracking and isomerization reactions. Ferrierite is actually used in such processes (as well as in several others involving e.g. isomerization), typically with high Si/Al ratios (from 8 to 27).[33] Because of its framework topology, characterized by restricted void spaces, this zeolite has an excellent transition state selectivity for such reactions. As the reaction occurs only on the external surface of the catalyst, at the pore entrances (“pore-mouth catalysis”),[33d] only a small fraction of the catalytic sites is actually exploited. On this basis, we might speculate that the application of moderate pressures could facilitate the entrance of the reactant molecules inside the zeolite channels, with probable beneficial effects on the catalytic process.

REFERENCES

(1) C. Baerlocher, L.B. McCusker, D.H. Olson, *Atlas of Zeolite Framework Types*, sixth ed., Elsevier, Amsterdam, **2007**.

(2) G. Gottardi, E. Galli, *Natural Zeolites*, Springer-Verlag, Berlin, 1985.

(3) W.S. Wise, R.W. Tschernich, *Am. Mineral*. **1976**, *61*, 60-66.

(4) H. Gies, R.P. Gunawardane, Zeolites **1987**, *7*, 442 – 445.

(5) A. Kuperman, S. Nadimi, S. Oliver, G. A. Ozin, J.M. Garces, M. M. Olken, *Nature* **1993**, *365*, 239 -242.

(6) P.A. Vaughan, *Acta Cryst*. **1966**, *21*, 983-990.

(7) A. Alberti, C. Sabelli, *Z. Kristallogr.* **1987**, *178*, 249-256.

(8) R.E. Morris, S.J. Weigel, N.J. Henson, L.M. Bull, M.T. Janicke, B.F. Chmelka, A.K. Cheetham, *J. Am. Chem. Soc.* **1994**, *116*, 11849-11855.

(9) a) R. Arletti, G. Vezzalini, S. Quartieri, F. Di Renzo, V. Dmitriev, *Microporous Mesoporous Mater.* **2014**, *191*, 27–3;. b) R. Gramlich-Meier, V. Gramlich, W. M. Meier, *Am. Mineral*. **1985**, *70*, 619-623.

(10) a) R. Miletich, D.R. Allan, W.F. Kush, in *High-pressure single-crystal techniques, High-Temperature and High-Pressure Crystal Chemistry*, *Reviews in Mineralogy and Geochemistry*, *Vol. 41*, (Eds: R. M. Hazen, R.T. Downs*),* Mineralogical Society of America and Geochemical Society, Chantilly, Virginia, **2000**, p. 445–519. b) R. J. Angel, M. Bujak, J. Zhao, G. D. Gatta, S. D. Jacobsen, *J. Appl. Cryst.* **2007***, 40*, 26-32.

(11) A. Yu. Likhacheva, Y. V. Seryotkin, A. Yu. Manakov, S. V. Goryainov, A. I. Ancharov, M. A. Sheromov, *Am. Mineral.* **2007**, *92*, 1610-1615.

(12) R.A. Forman, G. J. Piermarini, J.D. Barnett, S. Block, Science 1972, 176, 284–286.

(13) H.K. Mao, J. Xu, P.M. Bell, J. Geoph. Res. 1986, 91, 4673–4676.

(14) A. P. Hammersley, S. O. Svensson, M. Hanfland, A. N. Fitch, D. Häusermann, High Pressure Res.1996, 14, 235−248.

(14b) A. C. Larson, R. B. Von Dreele, General Structure Analysis System “GSAS”; Los Alamos National Laboratory Report; Los Alamos, 1994; LAUR 86-748.

(15) B.H. J. Toby, EXPGUI, a Graphical User Interface for GSAS. *J. Appl. Cryst.* **2001**, *34*, 210−213.

(16) P. Thomson, D.E. Cox, J.B. Hastings, *J. Appl. Cryst.* **1987**, *20*, 79–83.

(17) a) J. L. Jordá, F. Rey, G. Sastre, S. Valencia, M. Palomino, A. Corma, A. Segura, D. Errandonea, R. Lacomba, F. J. Manjón, O. Gomis, A. K. Kleppe, A. P. Jephcoat, M. Amboage, J. A. Rodríguez-Velamazán, *Angew. Chem. Int. Ed.* **2013**, *52*, 10458*; Angew. Chem*. **2013**, *125*, 10652; b) L. Gigli, R. Arletti, G. Tabacchi, E. Fois, J. G. Vitillo, G. Martra, G. Agostini, S. Quartieri, G. Vezzalini, *J. Phys. Chem. C* **2014**, *118*, 15732; c) G.D. Gatta,

G. Tabacchi, E. Fois, Y. Lee, *Phys. Chem. Minerals* **2016**, *43*, 209; d) M. Santoro, D. Scelta, K. Dziubek, M. Ceppatelli, F. A. Gorelli, R. Bini, G. Garbarino, J.-M. Thibaud, F. Di Renzo, O. Cambon, P. Hermet, J. Rouquette, A. van der Lee, J. Haines, *Chem. Mater*. **2016**, *28*, 4065.

(18) a) J. P. Perdew, K. Burke, M. Ernzerhof, *Phys. Rev. Lett.* **1996**, *77*, 3865–3868; b) S. Grimme, *J. Comput. Chem*. **2006**, *27*, 1787–1799.

(19) CPMD code, http://www.cpmd.org, Copyright IBM Corp. 1990–2016, MPI für Festkörperforschung Stuttgart 1997–2001.

(20) a) M. Fischer, F. O. Evers, F. Formalik, A. Olejniczak, *Theor. Chem. Acc.* **2016**, *135*, 257; b) M. Fischer, *Z Kristallogr.* **2015**, *230*, 325.

(21) D. Vanderbilt, *Phys. Rev. B* **1990**, *41*, 7892–7895

(22) L. Kleinman, D. M. Bylander, *Phys. Rev. Lett.* **1982**, *48*, 1425–1428.

(23) D. R. Hamman, M. Schlüter, C. Chiang, *Phys. Rev. Lett.* **1979**, *43*, 1494–1497.

(24) N. Troullier, J. L. Martins, *Phys. Rev. B* **1991**, *43*, 1993-2006.

(25) R. Car, M. Parrinello, *Phys. Rev. Lett*. **1985**, *55*, 2471-2474.

(26) a) R. A. Provencal, R. N. Casaes, K. Roth, J. B. Paul, C. N. Chapo, R.J. Saykally, *J. Phys. Chem. A* **2000**, *104*, 1423–1429; b) T.N. Wassermann, M. A. Suhm, *J. Phys. Chem. A* **2010**, *114*, 8223–8233; c) A. Vargas-Caamal, F. Ortiz-Chi, D. Moreno, A. Restrepo, G. Merino, J. L. Cabellos, *Theor. Chem. Acc.* **2015**, *134*,16.

(27) a) S. Nosé, *J. Chem. Phys*. **1984**, *81*, 511–519; b) W. G. Hoover, *Phys. Rev. A* **1985**, *31*,1695–1697.

(28) F. Cailliez, M. Trzpit, M. Soulard, I. Demachy, A. Boutin, J. Patarin, A. H. Fuchs, *Phys. Chem. Chem. Phys*. **2008**,*10*, 4817.

(29) G.D. Gatta, Y. Lee, *Mineral. Mag***. 2014**, *78*, 267

(30) F.-X. Coudert, F. Cailliez, R. Vuilleumier, A.H. Fuchs, A. Boutin, *Faraday Discuss*. **2009**, *141*, 377.

(31) S. R. G. Balestra, S. Hamad, A. R. Ruiz-Salvador, V. Domínguez−García, P. J. Merkling, D. Dubbeldam, S. Calero, *Chem. Mater*. **2015**, *27*, 5657.

(32) O. Ferro, S. Quartieri, G. Vezzalini, E. Fois, A. Gamba, G. Tabacchi, *Am. Mineral*. **2002**, *87*, 1415.

(33) a) A. Bonilla, D. Baudouin, J. Pérez-Ramírez, *J. Catal.* **2009**, *265*, 170; b) C. Martínez, A. Corma, *Coord. Chem. Rev.* **2011**, *255*, 1558; c) J. Čejka, G. Centi, J. Perez-Pariente, W. J. Roth, *Catal. Today* **2012**, *179*, 2; d) S. C. C. Wiedemann, Z. Ristanović, G. T. Whiting, V. R. Reddy Marthala, J. Kärger, J. Weitkamp, B. Wels, P. C. A. Bruijnincx, B. M. Weckhuysen, *Chem. Eur. J*. **2016**, *22*, 199.